*Journal of Imaging Science and Technology*® 55(1): 010505–010505-16, 2011.


# Improved Color Separation Based on Dot-Visibility Modeling and Color Mixing Rule for Six-Color Printers

**Chang-Hwan Son and Hyung-Min Park**
*Department of Electronic Engineering, Sogang University, R705, 1 Shinsu-dong, Mapo-gu, Seoul 121-742, Korea*

**Yeong-Ho Ha**▲
*School of Electrical Engineering and Computer Science, Kyungpook National University, 1370 Sankyuk-dong, Buk-gu, Daegu 702-701, Korea*
*E-mail: yha@ee.knu.ac.kr*

**Abstract.** *A method of converting cyan, magenta, yellow, and black (CMYK) digital values into cyan, magenta, yellow, black, light cyan, and light magenta (CMYKLcLm) in six-color printers is proposed for providing a better print quality with less dot visibility, high color fidelity, and smooth color transition. Based on the attribute of the dependent variable Lm and Lc to M and C, the input M and C digital values are separated into MYLm and CLcLm digital values, respectively, according to three types of region: bright, middle, and dark. In bright regions, the input M digital values are separated into LmY digital values minimizing the colorimetric errors to compensate for the hue difference between M and Lm, while C is separated into LcLm in the same manner. In middle regions, to guarantee a gradual lightness transition between bright and dark regions, M and C are newly included along with LmY and LcLm used in bright regions, respectively, which raises a redundancy problem, i.e., many to one mapping between M and MYLm or C and CLcLm. To solve this problem, a digital-patch-based dot visibility metric, which avoids the need to scan a large number of printed patches, is proposed based on the standard deviation of the lightness component for digitally bilevel patches through model-based error diffusion, thereby making it possible to choose the unique MYLm and CLcLm with the lowest dot visibility score. Finally, in dark regions, the input M and C digital values are modified by the M and C with the closest color to reduce the use of unnecessary amounts of colorant. Moreover, to eliminate the appearance of color tones on the gray ramp, the input gray CMY digital values are converted into CMYK digital values using a simple gray component replacement, and the input CMY digital values in the predefined gray boundary regions are then transformed by a weighted sum of the CMYLcLm obtained from above-mentioned color separation and the separated CMYK on the gray axis. Experimental results show that the proposed method is able to produce printed images with both a lower color difference and a lower dot visibility when compared to conventional methods. © 2011 Society for Imaging Science and Technology.*
[DOI: 10.2352/J.ImagingSci.Technol.2011.55.1.010505]

## INTRODUCTION

Cyan, magenta, yellow, black, light cyan, and light magenta (CMYKLcLm) printers represent a color by its vector in a six-dimensional color space. In reality, the vector corresponds to the C, M, Y, K, Lc, and Lm six-drive signals for controlling the amounts of their colorants and each element has 255 discrete levels in an 8-bit controlled digital color printer. However current imaging devices, cameras and scanners still represent an original color by its vector in a three-dimensional (3D) red-green-blue (RGB) color space, thereby breaking the one-to-one mapping between RGB and CMYKLcLm. The six-color separation is thus required to find the mapping function of transforming RGB into CMYKLcLm. Even though RGB can be directly converted into CMYKLcLm, the color management technology for converting RGB into CMY based on colorimetric color matching between cross-media has been accumulated and it is efficient and convenient to convert CMY into CMYKLcLm.[1] Above all, the reason why CMYKLcLm can be converted from CMY is that Lc, Lm, and K are the dependent variables of the C, M, and Y. Assuming that the Lc and Lm primaries have the same hues as the C and M primaries, but different degree of lightness, respectively, the C and M primaries can be expressed by the Lc and Lm primaries, thus creating the dependent relation between them. The black primary is also a dependent variable of the CMY primaries due to the possible gray reproduction by the mixture of the CMY colorants. It seems that the CMYKLcLm primaries form a six-dimensional color space, but the axes of Lc and Lm lie on those of the C and M in the CMY space. If the mixtures of C and Lc or M and Lm can create colors equal to C and M, certain amounts of the C and M primaries can be replaced by those of Lc and Lm to reproduce less visible dots. This replacement corresponds to the six-color separation of extracting the CMYKLcLm signals from the CMYK signals. The same explanation can be applied to the black colorant and the technique of extracting K from CMY is regarded as another field of color rendition, called gray component replacement (GCR).[2]

In CMYKLcLm printers, three degrees of freedom, equal to the number of extra colorants, can create the same tristimulus value from a different combination of colorants. This relationship raises the redundancy problem, wherein the combination of colorants should be selected for better image quality. Thus, in addition to the color difference, other

▲IS&T Member

Received Apr. 26, 2010; accepted for publication Sep. 25, 2010; published online Dec. 27, 2010.
1062-3701/2011/55(1)/010505/16/$20.00.

constraints such as dot visibility ordering, the total colorant limit, and the color constancy index may be considered to reduce the dot visibility, ink consumption, and metamerism. Many papers on this subject have been published, and two strategies have been used in six-color separation. The first approach attempts to convert the input C and M digital values with one dimension into (C and Lc) and (M and Lm) digital values. The advantages of this approach are that it is computationally less expensive and it can utilize commercial profile tools to make printer ICC profiles, where the relations between the Lab values and the CMYK values are defined based on a look-up table.[3]

Traditional six-color separation,[4] which uses the metric of the color difference, identifies monotonically increasing functions to convert M and C into (M and Lm) and (C and Lc) under the constraint of minimizing the color difference between them, respectively. Although an accurate colorimetric reproduction can be achieved, the image quality is inferior due to visible dots with cyan or magenta, especially in bright regions. As such, six-color separation using the subjective granularity and lightness values has also been proposed by Huang et al.[5] In their proposed method, the input C and M digital values are separated into the (C or Lc) and (M or Lm) digital values within an acceptable lightness difference and the granularity deviation. This method not only reduced the dot visibility on printed images with the use of only Lc and Lm in the bright regions but also decreased the abrupt difference in lightness from lighter to darker colors through the linearization of the input lightness value, although a significant color difference ensued due to the hue difference between the saturated (C, M) and diluted (Lc, Lm) colorants. In addition, the subjective granularity based on the visual examination score to quantify the degree of visual perception of dots on the printed patches may yield a fluctuating data distribution depending on the participants. To overcome these problems, Son et al. proposed the six-color separation using additional colorants and quantitative granularity metric, where the light magenta and yellow colorants were used in bright regions to correct the hue difference between the diluted and saturated colorants.[6] The six-color separation method of generating targeted photo-ink separation paths selected from combinations of diluted and saturated colorants is proposed under the constraints of ink-trapping and a smooth color transition.[7] Yet, since this method focuses on generating a target photo-ink separation path, the hue values for the input M and C inks may differ from those for the separated CLc or MLm colorants.

A second approach to convert CMY digital values into CMYLcLm digital values has been attempted. In Agar's method, a model-based printer characterization was used to reduce the number of measurement data, and the input CMY digital values were separated into CMYLcLm digital values to maximize the amounts of colorants in the order of Y, Lc, Lm, C, and M.[8] Here, accurate colorimetric reproduction and a smooth dot pattern can be simultaneously achieved, yet excessive amounts of colorants were used owing to the maximum use of colorants with lower dot visibility, which resulted in substrate wetness, increased drying time, and poor edge sharpness. Chen et al. proposed six-color separation to reduce the change in the perceived color under many different lighting conditions based on the index of color constancy.[9] The second approach mentioned above that converts 3D CMY into five-dimensional CMYLcLm may suffer from considerable computational requirements, in excess of the available memory, relatively inaccurate five-dimensional printer characterization compared to three-dimensional printer characterization, and additional handling of the total colorant limit and the edge sharpness.

Accordingly, this article proposes a method of separating one-dimensional C and M signals into CLcLm and MYLm signals. The proposed method is an updated version of our previous work.[6] While the fundamental idea remains the same, the main difference is the use of Y and Lm in both bright and middle regions to guarantee a smooth color transition. In the previous version, two types of colorant, Lc and C or Lm and M, are used in middle regions, whereas three types of colorant, Lc, C, and Lm or Lm, M, and Y are used in the present updated version. When Lc and Lm or Lm and Y are exchanged with Lc and C or Lm and M, respectively, at the borders of bright and middle regions, this can cause a sudden disappearance of the Lm and Y colorants in the boundary areas of middle regions, due to the absence of the Lm and Y colorants in middle regions in the case of six-color separation. In the previous work[6] the photo-ink separation paths had a very narrow range for middle regions, resulting in discontinuous color transitions between bright and middle regions. Thus, additional manual color-tuning was performed to correct this problem.

Therefore, to solve this problem, the updated version uses the Lm and Y colorants in middle regions. However, since the addition of Lm and Y to middle regions requires an increased number of printed patches for the dot visibility modeling and printer characterization, measurement-based printer characterization is changed to model-based printer characterization to reduce the amount of measurement data. In particular, the scanning-based dot visibility model used in the previous version is modified to a digital-based dot visibility model that does not require any printing or scanning processes. As a result, these modifications make it possible to use Lm and Y in middle regions and produce a sufficient number of LmMY and LcCLm candidates, thereby improving the six-color separation with a smooth color transition, less dot visibility, and accurate colorimetric reproduction. Another addition to the updated version is the generation of black to remove the appearance of color tones on the gray ramp. Thus, the gray-balanced CMY colorants are used with an amount of black colorant calculated using a simple GCR on the gray axis. The boundaries of the gray regions are established based on subjective experiments, and the amounts of the CMY colorants in those regions replaced by a weighted sum of CMYLcLm and CMYK. Meanwhile, in the other regions, the CMYLcLm colorants are only used to enhance the saturation and dot visibility

The remainder of this article is organized as follows.

The following section provides an overview of the proposed algorithm, followed by the detail explanation of the proposed method consisting of six subsections, i.e., digital generation, printer characterization, dot visibility modeling, six-color separation, black generation, and construction of look-up table are described. Then, the proposed method is compared with the conventional methods in the next section, and some conclusions are presented in the final section.

## OVERVIEW OF THE PROPOSED SIX-COLOR SEPARATION

The proposed method follows the basic scheme of our previous work in Ref. 6. However, there is a difference between the methods in that the additional colorants of the Y and Lm used in the bright regions are re-used in the middle regions to guarantee a smooth color transition. According to three types of regions, the used colorants are as follows:

$$f_{\mathrm{M}}(\mathrm{M}) = \begin{cases} \text{Lm and Y for } i=0 \\ \text{Lm, Y, and M for } i=1 \\ \text{M for } i=2 \end{cases} \quad f_{\mathrm{C}}(\mathrm{C}) = \begin{cases} \text{Lc and Lm for } i=0 \\ \text{Lc, Lm, and C for } i=1 \\ \text{C for } i=2, \end{cases} \tag{1}$$

where $f_{\mathrm{C}}$ and $f_{\mathrm{M}}$ designate the functions used for six-color separation of cyan and magenta, respectively. The value of $i(0,1,2)$ represents the three types of regions (bright, middle, and dark), and M, Lm, Y, C, and Lc indicate the kinds of colorants used. Specifically, Y and Lm, which are used in the bright region as output variables of $f_{\mathrm{M}}$ and $f_{\mathrm{C}}$, respectively, are called the additional colorants hereafter. In Eq. (1), it should be noted that the Y and Lm colorants are used for six-color separation in middle regions, which is in contrast to our previous work, where the Y and Lm colorants were only used in bright regions to correct the hue difference between diluted and saturated colorants. However, the addition of Lm and Y to middle regions requires an increased number of printed patches for the dot visibility modeling and printer characterization. Thus, the measurement-based printer characterization is changed to a model-based printer characterization in order to reduce the amount of measurement data. In particular, the scanning-based dot visibility model is also modified to a digital-based dot visibility model with no printing or scanning processes involved.

With the digital-based dot visibility modeling, many digital patches can be easily generated within the available memory using combinations of Lm, M, and Y or Lc, C, and Lm, and their dot visibility values can then be predicted based on model-based error diffusion and a SCIELAB conversion to make bilevel digital patches for use in a real printing environment, i.e., considering dot overlapping, and to apply low-pass filtering to the calculated *XYZ* values of the digital half-toned pixels. This modified dot visibility model

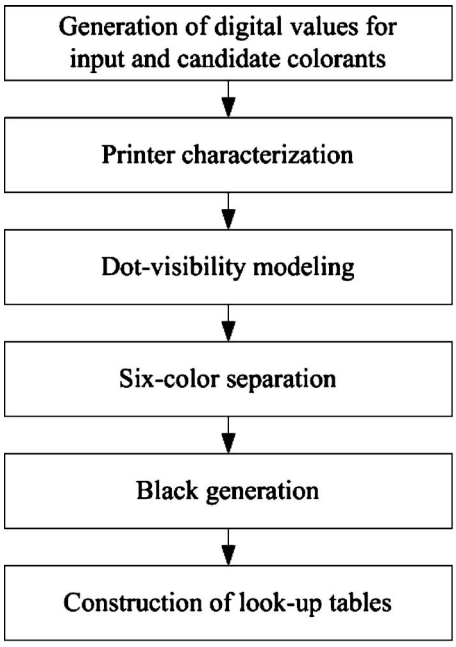


Figure 1. Flowchart for separating the CMY into the CMYKLcLm.

not only creates many MYLm and CLcLm candidates, but also avoids the time consuming printing and scanning of the MYLm and CLcLm patches.

For the printer characterization, an established model-based color mixing model, the Yule-Nielsen modified spectral Neugebauer (YNSN) model, is used to predict most of the CIELAB values for the MYLm and CLcLm candidates.[10] Since the proposed method follows the first approach, i.e., the conversion of C into three CLcLm candidates and M into three MYLm candidates, only eight measured Neugebauer primaries are required for the YNSN modeling, in contrast to other six-color separation methods, where four CMYK colorants are converted into six CMYKLcLm colorants, requiring 64 Neugebaurer primaries. Thus, if the same amount of measurement data is used for YNSN modeling, the proposed method can provide more accurate colorimetric reproduction than other six-color methods. The cellular-Yule-Nielsen-spectral-Neugebauer model can be also used to improve the performance of the printer characterization.[10]

The flowchart of the proposed method of converting the CMY digital value into the CMYKLcLm digital value is shown in Figure 1. First, the input digital values of cyan and magenta are sampled with equal step sizes. The digital values of the CLcLm and MYLm candidates are also generated by uniform sampling. Then, their spectral reflectances are estimated using model-based printer characterization to reduce the measurement data and transformed into tristimulus values by multiplying the relative daylight power distribution and a color matching function. In addition, dot visibility is quantitatively modeled based on the standard deviation of the lightness value in the SCIELAB color space to determine the degree of dot visibility of the candidates. Next, one or two constraints of the color difference and the dot visibility are imposed on all the candidates depending on the three

types of regions, and the final candidates are determined by minimizing the dot visibility or the color difference for each sampled input digital value, thus converting the input C and M digital values into CMYLcLm digital values. In addition, for better gray reproduction, the input digital values that belong to the predefined gray regions are transformed into the weighted sum of the separated CMYLcLm digital values and the CMYK digital values calculated by GCR. Lastly, three look-up tables for converting the CMY digital value into the CMYKLcLm digital value are constructed to reduce the computing time.

## GENERATION OF DIGITAL VALUES FOR INPUT AND CANDIDATE COLORANTS

The proposed method replaces the amounts of the input colorants with those of the CLcLm and MYLm colorants based on subtractive color mixing and the characteristics of dot visibility. Thus, the essential candidates are extracted from the combination of C, M, Y, Lc, and Lm for the input colorants. This approach enables a sufficient number of candidates to be generated and prevents the wastage of unnecessary colorants. Initially, to separate the C and M digital values into the CLcLm and MYLm digital values, the digital values of the input C and M colorants are sampled at $m$ intervals. When the sampling interval was less than 15, the CIE1976 color differences according to the 3D interpolations of the linear, prism, and tetrahedra were smaller than two,[11] the limit of human color discrimination.[12] Next, the digital values of the CLcLm and MYLm candidates are generated with uniform sampling. If the number of the candidates is small, an optimal candidate with a smaller color difference and less dot visibility can be excluded during the six-color separation. Thus, if possible, it is better to create all combinations of M, Y, and Lm or C, Lc, and Lm. The maximum number of MYLm and CLcLm candidates is $2^8 \times 2^8 \times 2^8$. Yet, in reality, the number of the candidates is restricted to the available memory, and it can be observed that the computer simulation stopped when the total number of candidates was about 2,500,000 on a 1 Gb RAM chip. Therefore, the sampling interval for each channel is set at two and generates the total number of 2,097,152 ($2^7 \times 2^7 \times 2^7$) combinations for each candidate.

## PRINTER CHARACTERIZATION

Depending on the printer devices, the digital values of the input and candidate colorants need to be converted into an independent color space through the printer characterization for accurate color reproduction. In addition, since increased amounts of colorants are used in multicolorant printers, an established model-based color mixing model of the YNSN model, is used to estimate the spectral reflectance of arbitrary printed patches based on the weighted average spectral reflectance of $2^N$ known basis colors, wherein $N$ is the number of colorants.[13] For CMY printers, the solid color overlays (i.e., 0% and 100% combinations) of C, M, and Y create eight basis colors: white, cyan, magenta, yellow, blue, green, red, and black. These basis colors are also known as the Neugebauer primaries in the YNSN model, as follows:

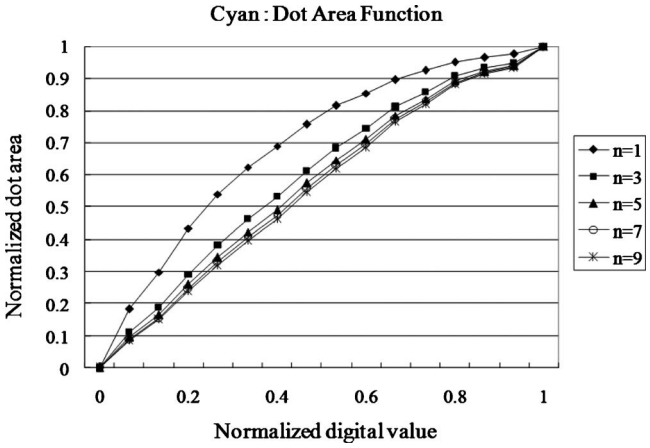


Figure 2. The cyan dot-area functions according to the Yule-Nielsen factor.

$$\hat{R}(\lambda) = \left[ \sum_{i=1}^{8} w_i(C,M,Y) P_i(\lambda)^{1/n} \right]^n, \qquad (2)$$

where λ indicates the wavelength in nanometer (nm) units, $\hat{R}(\lambda)$ is the estimated spectral reflectance with a range of 380 nm to 730 nm sampled by intervals of 10 nm, $P_i(\lambda)$ is the measured spectral reflectance corresponding to the $i$th Neugebauer primary, $w_i$ is the weight function of the relative dot area, and $n$ is the optical scattering factor or the Yule-Nielsen factor that accounts for the nonlinear relationship between the reflectance and the area coverage. In this article, the Demichel dot model wherein the locations of the CMY dots are statistically independent of the colorants[14] is assumed in order to calculate the weight function of the dot area and the eight combinations of (M, Y, Lm) and (C, Lc, Lm) are used as Neugebauer primaries in Eq. (2), instead of CMY primaries, as we merely focus on predicting the spectral reflectances of the MYLm and CLcLm candidates.

To find the dot area and the optical scattering factor, $w_i$ is initially optimized using the spectral regression method for a fixed $n$.[13] Next, with a fixed $w_i$, the optimal $n$ is determined by varying the $n$ parameter values and comparing the color difference for arbitrary color charts. Detailed explanation of estimating the dot area function can be found in Ref. 13. Even though the Yule-Nielsen $n$-factor has a physical meaning in region $1 < n < 2$, it can also be used as a free parameter to optimize the fit of the model to empirical data.[10,13] The spectral regression method only uses single-colorant samples to predict the dot area functions. Thus, to consider mixtures, e.g., neutral colorant samples, other dot area optimization in CIELAB color space can be used to improve the accuracy.

As an example, the cyan dot area functions according to the values of the Yule-Nielsen factor are shown in Figure 2. The estimated dot area functions are opposite to the tone response curve of the display with a gamma value, and they become linear as the Yule-Nielsen factor increases due to the consideration of the nonlinear factor that results mainly from the light scattering in that model. The parts of the

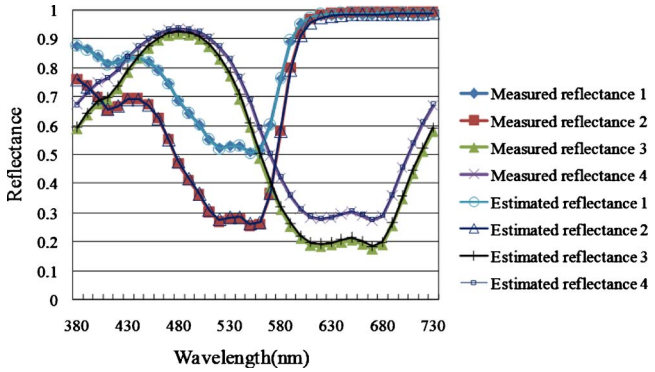


Figure 3. Comparison of the measured and estimated reflectances.

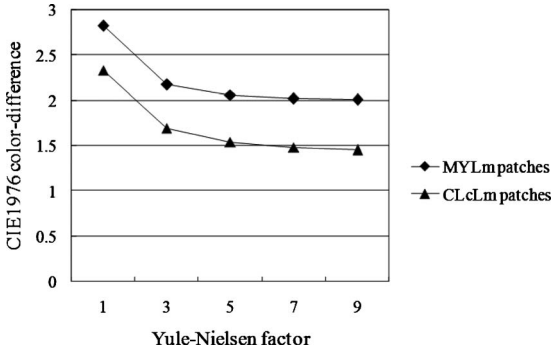


Figure 4. Color differences according to the values of Yule-Nielsen factor.

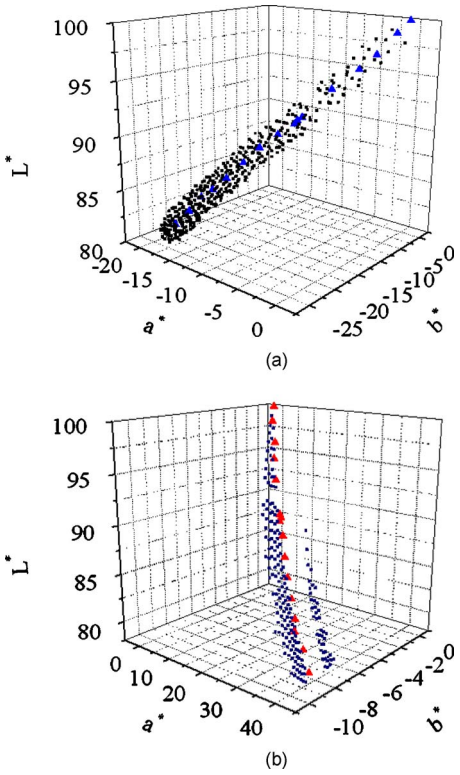


Figure 5. CIELAB values for some input and candidates; (a) C and CLcLm and (b) M and MYLm.

estimated and measured spectral reflectances for the input magenta and cyan are shown in Figure 3, and they are almost the same at each wavelength.

To evaluate the performance of the realized printer characterization, 64 test patches, generated via uniform sampling for each channel, are printed using scalar error diffusion, and then measured with a colorimeter. The CIE1976 color differences between the measured CIELAB values and the estimated CIELAB values are shown in Figure 4. They converge to a constant value if the value of the Yule-Nielsen factor reaches approximately nine, allowing for the use of any value above nine. In this article, the value of nine was used as the Yule-Nielsen factor. The average color difference for MYLm is slightly larger than that for CLcLm. Even though the scalar error diffusion used is a type of dot-on-dot printing, the estimated CIELAB values are accurate, and the assumption of the statistical independence of the printed dot location can be maintained well. It can be observed that on the printed image the misalignment of the dot location occurs due to mechanical error.

The estimated reflectances of the input and the candidates are transformed into CIEXYZ values by multiplying the relative spectral daylight power distribution and the color-matching function of the CIE 1931 standard colorimetric observer (2°) and then reconverted into the CIELAB values. The CIELAB values corresponding to the digital values of certain inputs and candidates are shown in Figure 5. The rectangles represent the CIELAB values of the MYLm and CLcLm candidates, respectively, and the red and blue triangles indicate the CIELAB values of the M and C inputs, respectively. In the case of the MYLm and CLcLm candidates, many CIELAB values can be mapped onto a rectangle according to the limited graphical expression in a commercial software tool. In fact, there are many candidate data around an input CIELAB value. From this figure, it is confirmed that the use of extra colorants can reproduce many of the same CIELAB values from the different combinations of the amounts of their colorants, and one-to-many mapping can exist between input data and the corresponding candidate data.

## DOT VISIBILITY MODELING

The same CIELAB values can be represented by different combined amounts of diluted and saturated colorants. In this case, the use of more saturated colorants can create a coarse dot-pattern due to the high dot visibility of saturated colorants, thereby degrading the image quality. Let us assume that there are two indistinguishable patches, as shown in Figure 6. Even if the color stimuli are the same, the degree of dot visibility of a half-tone color patch depends on the combination of the diluted and saturated colorants. The upper patch is printed with one color and it is not easy to detect the dots with good uniformity, whereas the bottom patch is formed from the combination of two colorants with different concentrations. This concentration deviation increases the dot visibility and creates coarse dot patterns. Thus, the upper patch is preferred rather than the bottom

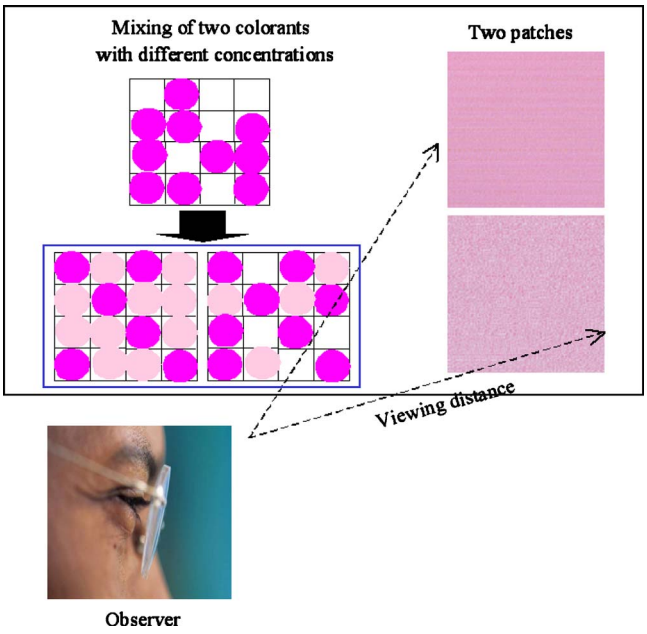


Figure 6. Necessity of dot visibility modeling in six-color separation.

patch in order to achieve higher quality image. The dot visibility of the half-toned color patches should be modeled to implement this preference. The visual observation shows that the degree of dot visibility of the half-tone patch is highly correlated with the standard deviation, which can be used to reflect both the visual perception of the lightness fluctuation and how visible the dots of the saturated colorant are relative to those of the diluted colorant. In addition, it is well known that dots tend to blur and integrate into a single color from an appropriate viewing distance.[15] The SCIELAB space includes the spatial-color sensitivity of the human eye to account for how a spatial dot pattern influences the color appearance. Accordingly, a quantitative dot visibility model is proposed based on the standard deviation of the lightness component in the SCIELAB color space. Moreover, this model is applied to a digitally half-toned image in order to avoid repetitive scanning of the printed MYLm and CLcLm candidates.

The block diagram for measuring the dot visibility of the half-tone patches is shown in Figure 7. First, the digital patches of the CLcLm and MYLm candidates are generated with an image size, and model-based error diffusion, reflecting the change in size of the printing dot, is applied to the digital patches to create bilevel images. Next, the CIEXYZ values of the digitally half-toned image are calculated at each pixel position from the measured data and then transformed into the SCIELAB space to convolute with the low-pass filtering function representing the human visual system. Finally, the degree of dot visibility of each patch is quantitatively defined as the standard deviation of the lightness value in the SCIELAB space. The acceptability of the proposed dot visibility metric is examined using a subjective rank order experiment, which asks an observer to arrange a given set of samples according to the increasing or decreasing magnitude of a particular perceptual attribute.[16]

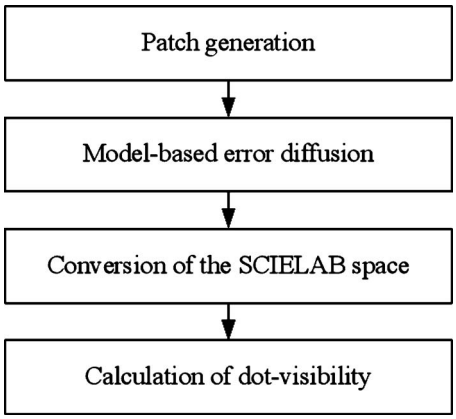


Figure 7. Block-diagram for measuring the dot visibility.

## PATCH GENERATION

In general, dot visibility prediction targets the printed patches scanned at high resolution to reflect the real dot distribution. However, the number of candidate patches to be printed on a high fidelity printer is too large, and thus digital patches with an image size $N \times N$ should be generated. The colors of the patches displayed on the RGB monitors are represented using the RGB colors. However, since RGB monitors do not have Lc and Lm drive signals, the colors of the digital MYLm and CLcLm patches are expressed using pseudo RGB colors on the RGB monitors. In other words, RGB colors are assigned in order to visualize the colors of the MYLm and CLcLm candidates on the RGB monitors, respectively. In addition, the digital patches have digital values that are equal to those used for the digital generation of the MYLm and CLcLm candidates.

## MODEL-BASED ERROR DIFFUSION

Assuming that the dpi (dot per inch) of the printer is the same as the ppi (pixel per inch) of the display and that the shape of a real dot is exactly square, without ink spreading, the produced tone levels correspond exactly to the number of the half-toned dots on the digital grid. However, conventional printers, such as dot matrix, ink-jet, and laser printers, have a circular dot shape due to the jaggedness and discontinuity that results from a square-shaped dot.[11] A circular shape will never exactly fit the size and shape of a square grid. The radii of the dots produced by a printer must be at least $T/\sqrt{2}$, wherein $T$ is the spacing of the Cartesian grid, so that a page may be blackened entirely. The dots will overlap, and the dot will become enlarged due to the spreading of the ink, thus breaking the linear gray tone reproduction. To find the degree of the overlapped area between adjacent dots, the circular dot overlap model has been developed.[17,18] This model assumes an ideal round shape with a fixed size and a constant absorptance. The overlapping areas are computed using geometric relationships, especially in terms of three area parameters ($\alpha$, $\beta$, and $\gamma$) which can be expressed in terms of the ratio $\rho$ of the actual dot radius to the minimum dot radius $T/\sqrt{2}$, as follows:

**Table I.** Measured CIEXYZ values for MYLm primaries.

| | M | Y | Lm | X | Y | Z |
|---|---|---|---|---|---|---|
| 0 | 255 | 255 | 255 | 94.9 | 100 | 108.5 |
| 1 | 255 | 255 | 0 | 62.4 | 42.3 | 58.9 |
| 2 | 255 | 0 | 255 | 74.4 | 78.4 | 9.04 |
| 3 | 0 | 255 | 255 | 45.2 | 24.1 | 26.8 |
| 4 | 0 | 0 | 0 | 39.6 | 22.8 | 6.34 |
| 5 | 255 | 0 | 0 | 52 | 38.5 | 7.6 |
| 6 | 0 | 0 | 255 | 40.1 | 23.5 | 5.3 |
| 7 | 0 | 255 | 0 | 42.9 | 22.6 | 23.2 |

**Table II.** Measured CIEXYZ values for CLcLm primaries.

| | C | Lc | Lm | X | Y | Z |
|---|---|---|---|---|---|---|
| 0 | 255 | 255 | 255 | 94.9 | 100 | 108.5 |
| 1 | 255 | 255 | 0 | 62.7 | 42.6 | 59.3 |
| 2 | 255 | 0 | 255 | 34.8 | 48.9 | 91.3 |
| 3 | 0 | 255 | 255 | 17.4 | 24.7 | 67.8 |
| 4 | 0 | 0 | 0 | 12.3 | 12.5 | 45.7 |
| 5 | 255 | 0 | 0 | 21.9 | 19.3 | 54.5 |
| 6 | 0 | 0 | 255 | 15.6 | 22.1 | 62.8 |
| 7 | 0 | 255 | 0 | 12.2 | 11.8 | 45 |

$$\alpha = \frac{1}{4}\sqrt{2\rho^2 - 1} + \frac{\rho^2}{2}\sin^{-1}\left(\frac{1}{\sqrt{2}\rho}\right) - \frac{1}{2},$$

$$\beta = \frac{\pi\rho^2}{8} - \frac{\rho^2}{2}\sin^{-1}\left(\frac{1}{\sqrt{2}\rho}\right) - \frac{1}{4}\sqrt{2\rho^2 - 1} + \frac{1}{4},$$

$$\gamma = \frac{\rho^2}{2}\sin^{-1}\left(\sqrt{\frac{\rho^2 - 1}{\rho^2}}\right) - \frac{1}{2}\sqrt{\rho^2 - 1} - \beta. \qquad (3)$$

In this article, the optimal value of $\rho$ is determined by finding the minimum sum of the absolute errors between the measured and estimated lightness values of the step wedge patches.

$$\rho^* = \arg\min_{\rho}\left[E = \sum_{k=0}^{M} |EL_k(\rho) - ML_k|\right], \quad k = 0, 1, \ldots, M, \qquad (4)$$

where $E$ indicates the sum of the absolute lightness error; $EL_k$ and $ML_k$ are the estimated and measured lightness values corresponding to $k$th step wedge patch. $M$ indicates the total number of step wedge patches, which is 16 based on uniform sampling at intervals of 17 for each C, M, Y, Lc, and Lm. The values of $\rho$ are changed from the minimum = 1.0 to the maximum = 1.414 at intervals of 0.1. In Eq. (4), the lightness values of $ML_k$ are obtained by measuring the CIELAB values of the step wedge patches, while the lightness values, $EL_k$, are estimated by half-toning the digital step wedge patches through the mode-based error diffusion using the circular dot overlap model[18] and then calculating by dividing the sum of the lightness values at all pixel positions by the patch size. Originally, model-based error diffusion has been proposed to correct nonlinear tone reproduction. This is opposite, however, to our goal of generating a pattern of pixels on a digital grid similar in tone characteristics to a real half-tone image. Thus, an input grayscale image in Ref. 18 should be inverted for achieving this purpose;

$$EL_k = \frac{1}{N^2}\sum_{i}^{N}\sum_{j}^{N} L(b_{i,j}), \qquad (5)$$

where $L(b_{i,j})$ indicates the lightness value corresponding to the bileveled pixel $b_{i,j}$ at the pixel position $(i,j)$ that belongs to $k$th digitally half-toned step of the step wedge, with an image size of $N^2$, and it can take one of the eight lightness values corresponding to the (M, Y, and Lm) or (C, Lc, and Lm) combinations with bilevels 0 or 255. The measured eight CIEXYZ values corresponding to the eight digital values are shown in Tables I and II. These CIEXYZ values are

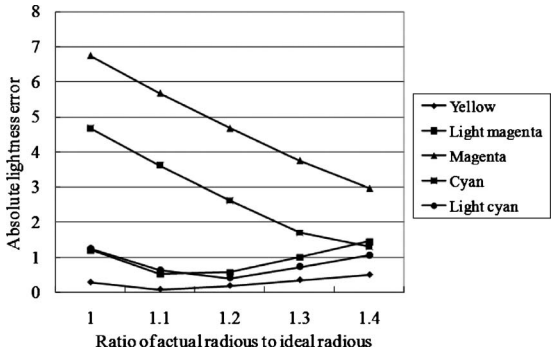


Figure 8. Absolute lightness errors according to the values of $\rho$.

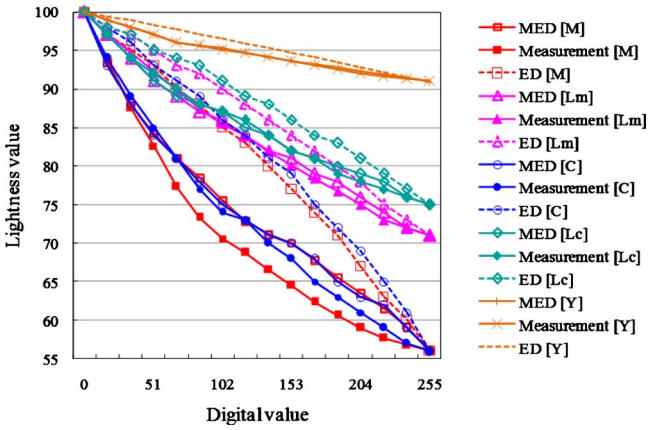


Figure 9. Comparison of the estimated and measured lightness values for M, Lm, C, Lc, and Y.

converted into the CIELAB values with a uniform color difference, and the lightness values are used as $L(b_{i,j})$ in Eq. (5).

The average absolute lightness errors, according to the values of $\rho$ for C, M, Y, Lc, and Lm, are shown in Figure 8. The Y, Lc, and Lm with light concentrations have the lower average absolute lightness errors than the C and M with dark concentrations. Moreover, the optimal values of $\rho$ for the minimization of the errors are smaller than those of C and M. This is because the dark concentration results in a high incidence of ink-spreading, which increases the dot size. Especially, from the absolute lightness error, the circular dot overlap model does not work well for magenta due to the excessively overlapping areas. The optimal values of $\rho$ are determined as 1.4, 1.4, 1.1, 1.2, and 1.1 for C, M, Y, Lc, and Lm, respectively. A comparison of the estimated and measured lightness values is shown in Figure 9 for C, M, Y, Lc, and Lm. In Fig. 9, ED indicates the conventional error diffusion using a Stucki error filter, and MED indicates the model-based error diffusion. ED produces the relatively linear tone response curve, yet this is very different from the measured nonlinear data. MED considers the dot overlap between adjacent dots and makes the nonlinear tone response curve similar to the measured data.

## CONVERSION OF THE SCIELAB COLOR SPACE

To calculate the dot visibility of one half-toned digital patch, it is necessary to calculate the CIEXYZ value corresponding to $b_{i,j}$ at a pixel position. This can easily be done by choosing the CIEXYZ value from the eight measured CIEXYZ values in Tables I and II. In addition, these CIEXYZ values should be transformed into the SCIELAB color space to reflect the low-pass filtering of the human eye. This phenomenon can be observed in real printed half-tone images, wherein dots tend to blur and integrate into a single color from an appropriate viewing distance. However, while the CIE1976 color difference is suitable for use on large uniform color targets, it is not appropriate for images, as color sensitivity changes as a function of spatial patterns. Zhang and Wandell proposed a spatial extension to CIELAB to account for how spatial patterns influence color appearance and color discrimination.[15] Thus, to reflect the contrast sensitivity function of the human visual system, a spatial filtering is added in SCIELAB space that is performed in an opponent-color space consisting of one luminance and two chrominance signals. The opponent signals, AC1C2, can be obtained through a linear transformation from CIE1931 $XYZ$;[19]

$$\begin{bmatrix} A \\ C_1 \\ C_2 \end{bmatrix} = \begin{bmatrix} 0.297 & 0.72 & -0.107 \\ -0.449 & 0.29 & -0.077 \\ 0.086 & -0.59 & 0.501 \end{bmatrix} \begin{bmatrix} X \\ Y \\ Z \end{bmatrix}. \quad (6)$$

After the CIEXYZ values are transformed into the opponent color space, the independent channels are spatially filtered using a series of convolutions in the spatial domain. SCIELAB color space uses two-dimensional convolution kernels, which are unit sum kernels, in the form of a series of Gaussian functions. The luminance filter has a narrow spread in the spatial domain, whereas the R-G and B-Y channels have relatively wide spreads. If the spatial filters are transformed into the frequency domain using a discrete Fourier transform, the luminance filter will have a wider bandwidth than the chrominance filters, as the Gaussian filter can be an impulse function with all frequencies by narrowing the spread of the filter. This means that the luminance sensitivity of the human eye is more sensitive to high frequencies than the chrominance sensitivity.

## CALCULATION OF THE DOT VISIBILITY

The filtered images are reconverted into the CIEXYZ values using the inverse matrix from Ref. 19 and then back into the CIELAB values. The standard deviation in the lightness channel is calculated and defined as the dot visibility value of each digital patch image;

$$DV_m = \sqrt{\frac{\sum_i \sum_j (L_{i,j} - L_{\text{mean}})^2}{N^2}} \quad \text{for } m = 0,1,\ldots,2,097,152, \quad (7)$$

where $L_{i,j}$ is the lightness value at the spatial coordinate $(i,j)$, $L_{\text{mean}}$ is the average lightness value, and $m$ is total patch number assigned to the MYLm or CLcLm candidates. $N^2$ and $DV_m$ are the pixel number and the dot visibility value,

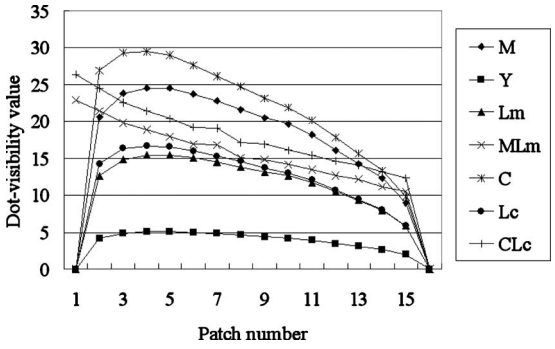


Figure 10. Estimated dot visibility values for test patches.

respectively. The printed step wedges, including C, M, Y, Lc, Lm, CLc, and MLm, are used as testing patches to calculate the dot visibility values. The sampling interval for each step wedge patch is 17, and the CLc and MLm patches are made by increasing the digital values of Lc and Lm with the sampling intervals, while fixing the digital values of C and M at 100. The estimated dot visibility values of test patches are shown in Figure 10. Among the C, M, Y, Lc, and Lm patches, the yellow colorant has the smallest dot visibility value and the cyan colorant has the largest value. The magnitudes of the dot visibility values of the colorants are highly correlated with their lightness values. The dots of Lc, Lm, and Y with high lightness are relatively less visible than those of C and M with low lightness. In the case of the C and M colorants, even though the lightness value of the magenta colorant is almost the same as that of the cyan colorant, as shown in Fig. 9, the opponent color transformation imposes higher weights for the R and G channels, more than for the $Z$ channel, to get the luminance channel. Thus, the lightness value of the cyan colorant becomes lower than that of the magenta colorant. This reflects that the green channel considerably influences the degree of lightness perceived by the human eye. In addition, for each colorant, the dot visibility value peaks at around the patch number of five and tends to decrease as the patch number increases. When the patch number approaches zero, indicating a white patch, it is not easy for the human eye to find dots on the printed patch. On the contrary, as the patch number approaches 16, the patches become uniform and covered with one color. Thus, the dots cannot be detected by the human eye. However, the dot visibility values become large when the dots are properly printed on paper. In other words, when the spacing between the printed dots, i.e., the frequency of the dots, is very narrow or very wide, the dot visibility values decrease. This result shows that the envelope of the estimated dot visibility is correlated with that of the contrast sensitivity function of the human eye. For the CLc and MLm patches, the dot visibility values become smaller as the amounts of the diluted colorants increase. This tells us that the amounts of the diluted colorants are a decisive factor in reducing dot visibility.

To evaluate the proposed dot visibility model, a subjective rank order experiment,[16] which asks the observer to arrange a given set of samples according to increasing or decreasing magnitudes of a particular perceptual attribute, is initially separately conducted for C, M, Lc, Lm, MLm, and CLc. Six digital imaging experts aged 27 to 32 participated in the experiment, and the yellow colorant was excluded from the test patches because its dots are only marginally visible to the human eye. Similarly, the estimated ranks are assigned to C, M, Lc, Lm, MLm and CLc and compared with the calculated dot visibility values. Then, the correlation factor [Eq. (8)] is used to measure the similarity between the estimated and measured dot visibility ranks;

$$\rho = \frac{\sum_{k=1}^{M} ER_k \cdot MR_k}{\sqrt{\sum_{k=1}^{M} ER_k^2}\sqrt{\sum_{k=1}^{M} MR_k^2}} \quad k = 0,1,\ldots,M, \qquad (8)$$

where $ER_k$ and $MR_k$ indicate the estimated and measured ranks, respectively, for $k$th step wedge patch. $M$ indicates the total number of step wedge patches, and its value is given by 16 based on uniform sampling with intervals of 17 for each C, M, Lc, Lm, MLm, and CLc. In general, if the average correlation factor is larger than about 0.90, the proposed model can be recommended as an acceptable metric.[20] The results of the rank and correlation for the testing patches are shown in Table III, in which *ER* and *MR* (1, 2, 3, 4, 5, and 6) represent the estimated rank and the measured ranks of six observers, respectively. For the testing patches, the average correlation factor values are all higher than 0.90, and the average correlation values for the diluted colorants are smaller than those of the saturated colorants. It seems that some observers are not able to assign ranks for the Lc and Lm patches with relatively invisible dots. In addition, the observers give the higher ranks for patches 2 and 5 and assigned lower ranks to the other patches. This tendency agrees with the results of the estimated dot visibility ranks. It is thus concluded that the proposed dot visibility model can be used as a new metric.

## SIX-COLOR SEPARATION

The block-diagram for converting the digital values of the input C and M colorants into the digital values of the MYLm and CLcLm candidates is shown in Figure 11. Initially, the input digital value ($x$) is zero, indicating the white paper without dots. The value of the decision factor ($i$) for discriminating the three types of regions is also set at zero, which indicates a bright region. Then, as many digital values as possible of the CLcLm or MYLm candidates are generated to guarantee a sufficient number of candidates that correspond to the input digital value. Their CIELAB values are estimated using the YNSN color mixing model to achieve color consistency between the input colorant and the candidate. In addition, the dot visibility values of the candidates are quantitatively calculated with the proposed dot visibility metric to recommend the candidate with the lowest dot visibility. Next, the initial digital value ($x$) is separated into the digital values ($k$,$j$) of the additional and diluted colorants to

**Table III.** Evaluation of the proposed dot visibility model.

| | Patch number | 1 | 2 | 3 | 4 | 5 | 6 | 7 | 8 | 9 | 10 | 11 | 12 | 13 | 14 | 15 | 16 | Correlation factor |
|---|---|---|---|---|---|---|---|---|---|---|---|---|---|---|---|---|---|---|
| M | ER | 16 | 7 | 3 | 1 | 2 | 4 | 5 | 6 | 8 | 9 | 10 | 11 | 12 | 13 | 14 | 15 | |
| | MR 1 | 16 | 4 | 3 | 2 | 1 | 5 | 6 | 7 | 8 | 9 | 10 | 11 | 12 | 13 | 14 | 15 | 0.9953 |
| | MR 2 | 16 | 1 | 4 | 3 | 2 | 9 | 6 | 5 | 7 | 8 | 10 | 11 | 12 | 13 | 14 | 15 | 0.9765 |
| | MR 3 | 16 | 4 | 3 | 1 | 2 | 7 | 5 | 6 | 8 | 9 | 10 | 11 | 12 | 13 | 14 | 15 | 0.9939 |
| | MR 4 | 16 | 1 | 2 | 3 | 4 | 6 | 5 | 7 | 9 | 10 | 11 | 8 | 12 | 13 | 14 | 15 | 0.9792 |
| | MR 5 | 16 | 6 | 3 | 2 | 1 | 4 | 5 | 7 | 8 | 9 | 10 | 11 | 12 | 13 | 14 | 15 | 0.9986 |
| | MR 6 | 16 | 2 | 6 | 7 | 1 | 5 | 3 | 8 | 10 | 11 | 12 | 4 | 13 | 14 | 9 | 15 | 0.9438 |
| | | | | | | | | Average correlation value | | | | | | | | | | 0.9812 |
| C | Patch number | 1 | 2 | 3 | 4 | 5 | 6 | 7 | 8 | 9 | 10 | 11 | 12 | 13 | 14 | 15 | 16 | Correlation factor |
| | ER | 16 | 5 | 2 | 1 | 3 | 4 | 6 | 7 | 8 | 9 | 10 | 11 | 12 | 13 | 14 | 15 | |
| | MR 1 | 16 | 4 | 3 | 2 | 1 | 5 | 6 | 7 | 8 | 9 | 10 | 11 | 12 | 13 | 14 | 15 | 0.9953 |
| | MR 2 | 16 | 1 | 5 | 4 | 2 | 10 | 8 | 7 | 9 | 11 | 14 | 3 | 12 | 13 | 6 | 15 | 0.9251 |
| | MR 3 | 16 | 4 | 2 | 1 | 3 | 8 | 6 | 5 | 10 | 9 | 11 | 7 | 14 | 13 | 12 | 15 | 0.9832 |
| | MR 4 | 16 | 1 | 2 | 3 | 4 | 7 | 5 | 6 | 9 | 10 | 11 | 8 | 13 | 14 | 12 | 15 | 0.9832 |
| | MR 5 | 16 | 6 | 4 | 1 | 2 | 3 | 5 | 7 | 8 | 9 | 10 | 11 | 12 | 13 | 14 | 15 | 0.9973 |
| | MR 6 | 16 | 2 | 9 | 10 | 1 | 11 | 7 | 4 | 6 | 8 | 12 | 3 | 13 | 14 | 5 | 15 | 0.9431 |
| | | | | | | | | Average correlation value | | | | | | | | | | 0.9712 |
| Lc | Patch number | 1 | 2 | 3 | 4 | 5 | 6 | 7 | 8 | 9 | 10 | 11 | 12 | 13 | 14 | 15 | 16 | Correlation factor |
| | ER | 16 | 5 | 2 | 1 | 3 | 4 | 6 | 7 | 8 | 9 | 10 | 11 | 12 | 13 | 14 | 15 | |
| | MR 1 | 16 | 4 | 3 | 2 | 1 | 5 | 6 | 7 | 8 | 9 | 10 | 11 | 12 | 13 | 14 | 15 | 0.9919 |
| | MR 2 | 16 | 1 | 6 | 5 | 2 | 11 | 8 | 7 | 10 | 9 | 14 | 3 | 12 | 13 | 4 | 15 | 0.8911 |
| | MR 3 | 16 | 4 | 3 | 2 | 1 | 7 | 6 | 5 | 8 | 10 | 11 | 9 | 12 | 13 | 14 | 15 | 0.9859 |
| | MR 4 | 16 | 1 | 2 | 4 | 3 | 6 | 5 | 7 | 9 | 10 | 11 | 8 | 12 | 14 | 13 | 15 | 0.9705 |
| | MR 5 | 16 | 7 | 4 | 1 | 2 | 3 | 5 | 6 | 8 | 9 | 10 | 11 | 12 | 13 | 14 | 15 | 0.9986 |
| | MR 6 | 16 | 3 | 8 | 14 | 1 | 6 | 13 | 5 | 7 | 11 | 12 | 2 | 9 | 10 | 4 | 15 | 0.8441 |
| | | | | | | | | Average correlation value | | | | | | | | | | 0.9470 |
| Lc | Patch number | 1 | 2 | 3 | 4 | 5 | 6 | 7 | 8 | 9 | 10 | 11 | 12 | 13 | 14 | 15 | 16 | Correlation factor |
| | ER | 16 | 7 | 3 | 1 | 2 | 4 | 5 | 6 | 8 | 9 | 10 | 11 | 12 | 13 | 14 | 15 | |
| | MR 1 | 16 | 4 | 3 | 2 | 1 | 5 | 6 | 7 | 8 | 9 | 10 | 11 | 12 | 13 | 14 | 15 | 0.9953 |
| | MR 2 | 16 | 1 | 8 | 7 | 2 | 10 | 5 | 4 | 11 | 12 | 14 | 3 | 13 | 9 | 6 | 15 | 0.8943 |
| | MR 3 | 16 | 4 | 3 | 1 | 2 | 6 | 7 | 5 | 10 | 8 | 9 | 11 | 12 | 13 | 14 | 15 | 0.9919 |
| | MR 4 | 16 | 1 | 2 | 3 | 4 | 7 | 6 | 5 | 9 | 10 | 11 | 8 | 13 | 14 | 12 | 15 | 0.9752 |
| | MR 5 | 16 | 7 | 3 | 1 | 2 | 4 | 5 | 6 | 8 | 9 | 10 | 11 | 12 | 13 | 14 | 15 | 1 |
| | MR 6 | 16 | 2 | 9 | 10 | 1 | 11 | 7 | 4 | 6 | 8 | 12 | 3 | 13 | 14 | 5 | 15 | 0.8811 |
| | | | | | | | | Average correlation value | | | | | | | | | | 0.9563 |

minimize the colorimetric error. Then, $x$ increases at the sampling intervals of $m$, and the above-mentioned steps are repeated until the digital value of the diluted colorant reaches the predefined maximum value. At this time, the lightness monotonicity constraint should have been guaranteed, and the digital value of the separated diluted colorant should have been forcibly increased to obtain the desired photo-ink separation paths.

For printer systems controlled by an eight bit-depth, the input cyan colorant can have a maximum digital value of 255 to fully utilize the amount of the light cyan. Namely, until the lightness value of the input cyan is lower than the minimum lightness value of light cyan, only light cyan is used instead of cyan to minimize dot visibility. For the magenta colorant, the amount of light magenta separated from the input cyan colorant are added to that of the light ma-

**Table III.** (*Continued.*)

| | Patch number | 1 | 2 | 3 | 4 | 5 | 6 | 7 | 8 | 9 | 10 | 11 | 12 | 13 | 14 | 15 | 16 | Correlation factor |
|---|---|---|---|---|---|---|---|---|---|---|---|---|---|---|---|---|---|---|
| MLm | Patch number | 1 | 2 | 3 | 4 | 5 | 6 | 7 | 8 | 9 | 10 | 11 | 12 | 13 | 14 | 15 | 16 | Correlation factor |
| | ER | 1 | 2 | 3 | 4 | 5 | 6 | 7 | 8 | 9 | 10 | 11 | 12 | 13 | 14 | 15 | 16 | |
| | MR 1 | 2 | 1 | 3 | 4 | 5 | 6 | 7 | 8 | 9 | 10 | 11 | 12 | 13 | 14 | 15 | 16 | 0.9993 |
| | MR 2 | 1 | 2 | 3 | 4 | 5 | 6 | 7 | 8 | 9 | 10 | 11 | 12 | 13 | 14 | 15 | 16 | 1 |
| | MR 3 | 5 | 3 | 4 | 1 | 2 | 6 | 7 | 8 | 9 | 10 | 11 | 12 | 13 | 14 | 15 | 16 | 0.9879 |
| | MR 4 | 1 | 2 | 3 | 4 | 5 | 6 | 7 | 8 | 9 | 10 | 11 | 12 | 13 | 14 | 15 | 16 | 1 |
| | MR 5 | 2 | 1 | 3 | 4 | 7 | 6 | 8 | 5 | 9 | 10 | 11 | 12 | 13 | 14 | 15 | 16 | 0.9946 |
| | MR 6 | 1 | 2 | 3 | 4 | 5 | 6 | 7 | 8 | 9 | 10 | 11 | 12 | 13 | 14 | 15 | 16 | 0.9997 |
| | | | | | | | Average correlation value | | | | | | | | | | | 0.9968 |
| CLc | Patch number | 1 | 2 | 3 | 4 | 5 | 6 | 7 | 8 | 9 | 10 | 11 | 12 | 13 | 14 | 15 | 16 | Correlation factor |
| | ER | 1 | 2 | 3 | 4 | 5 | 6 | 7 | 8 | 9 | 10 | 11 | 12 | 13 | 14 | 15 | 16 | |
| | MR 1 | 2 | 1 | 3 | 4 | 5 | 6 | 7 | 8 | 9 | 10 | 11 | 12 | 13 | 14 | 15 | 16 | 0.9993 |
| | MR 2 | 2 | 1 | 3 | 4 | 5 | 7 | 6 | 9 | 8 | 10 | 13 | 11 | 12 | 14 | 15 | 16 | 0.9959 |
| | MR 3 | 6 | 1 | 2 | 3 | 4 | 5 | 7 | 8 | 9 | 10 | 11 | 12 | 13 | 14 | 15 | 16 | 0.9899 |
| | MR 4 | 2 | 1 | 3 | 4 | 5 | 6 | 7 | 8 | 9 | 10 | 11 | 12 | 13 | 14 | 15 | 16 | 0.9993 |
| | MR 5 | 1 | 2 | 3 | 7 | 8 | 4 | 5 | 6 | 9 | 10 | 11 | 12 | 13 | 14 | 15 | 16 | 0.9899 |
| | MR 6 | 1 | 2 | 3 | 4 | 5 | 6 | 7 | 9 | 8 | 10 | 11 | 12 | 13 | 14 | 15 | 16 | 0.9993 |
| | | | | | | | Average correlation value | | | | | | | | | | | 0.9952 |

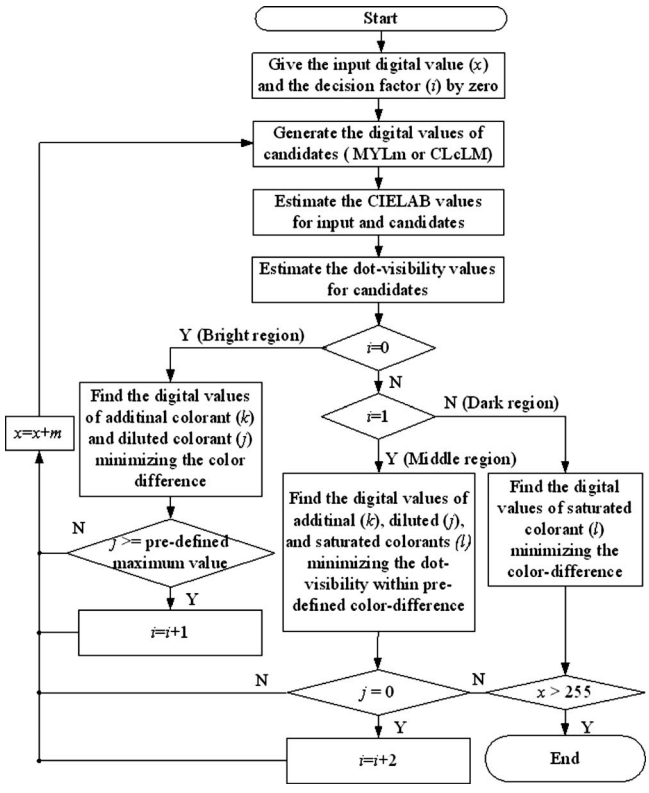


Figure 11. Block-diagram of the proposed six-color separation.

genta separated from the input magenta colorant to form CMYLcLm from MYLm and CLcLm. Thus, the summed digital value of light magenta can exceed the maximum digital value. To prevent clipping, the maximum digital value of the light magenta separated from the input cyan is subtracted from the maximum digital value, and the difference is used as the predefined maximum value of light magenta. If the digital value of the diluted colorant is smaller than the predefined maximum value, the input C or M digital value belong to a bright region. Otherwise, the decision factor increases by one, indicating that the next input digital value belongs to a middle region. Then, the CIELAB values and the dot visibility values for the input colorant and the candidates are iteratively calculated, and the input digital value is separated into the digital values $(k,j,l)$ of MYLm or CLcLm, thereby minimizing the dot visibility value within the acceptable color difference value of two until the digital value of the diluted colorant reaches zero. At this time, the digital value of the diluted colorant is forcibly decreased, and the digital value of the saturated colorant is forcibly increased due to the ineffectiveness of the diluted colorant. The more the input digital value increases, the more the white paper is covered with dots. This forms a uniform patch with low dot visibility, which decreases the effectiveness of the diluted colorant. When the digital value of the diluted colorant reaches zero, indicating the dark region, the decision factor increases by one and the input digital value is separated into the digital value $(l)$ of only the saturated

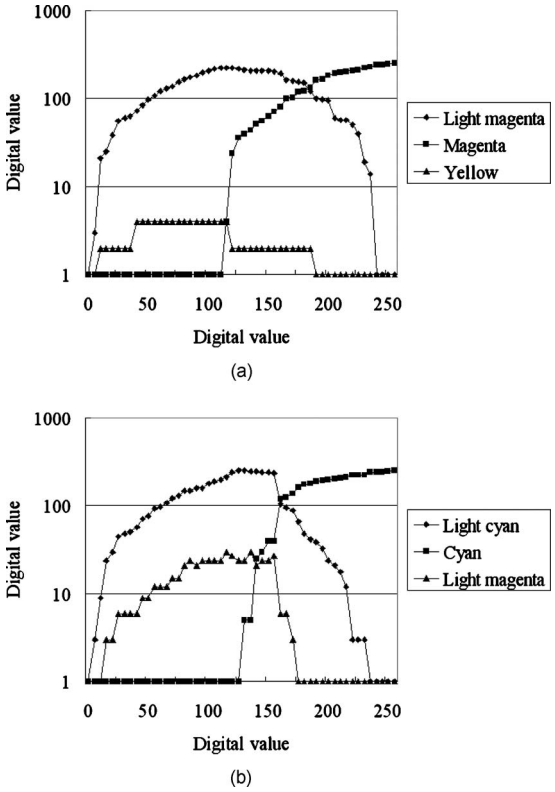


Figure 12. Proposed photo-ink separation paths; (a) magenta and (b) cyan.

colorant minimizing their color difference. In the dark region, the dot areas are fully printed with one color of cyan or magenta. Thus, the dot visibility cannot be reduced when a diluted colorant is added to a saturated colorant. The use of the diluted colorant only increases ink consumption and drying time in that region. The above-mentioned processes will be stopped if the input digital value reaches 255.

The photo-ink separation paths resulting from the proposed six-color separation method for the magenta and cyan colorants are shown in Figure 12. The abscissa axis represents the input digital value, and the ordinate axis represents the separated digital value scaled by the logarithm function, due to the small value of the additional colorant. In addition, the separated digital values with zero are artificially mapped onto those with one for the graphical expression in the log space. As seen, the separation paths are classified into three types of regions, and three kinds of colorants are used. In the bright regions, a small amount of an additional colorant (light magenta or yellow) is already sufficient to produce accurate colorimetric reproduction. In the middle regions, the (M, Y, or Lm) or (C, Lc, or Lm) combination is used, and in the dark regions, only cyan or magenta is used. Using these photo-ink separation paths, the input CMY can be separated into CMYLcLm.

## BLACK GENERATION

The input CMY digital values have been converted into the CMYLcLm digital values to improve dot visibility and yield smooth dot patterns. However, in the highlight regions,

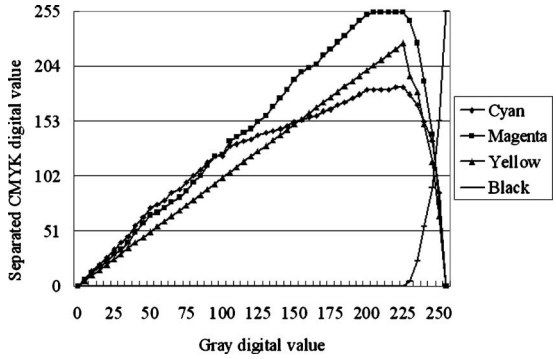


Figure 13. Separation paths for gray axis.

most of the CMY colorants are replaced with the LcLmY colorants with lower digital values, according to the lightness monotonicity constraint. The yellow colorant requires excessive amounts of the Lc and Lm colorants to create the same gray color made from the CMY digital value. Thus, the mixing of LcLm, LmY, and Y may destroy the gray-balancing with an appearance of a color tone. On the gray axis, the amounts of the CMYK colorants are replaced by those of the separated CMYLcLm colorants for better gray reproduction. Initially, the amounts of the CMY colorants are balanced by varying the digital values of only cyan and magenta at a fixed value of yellow, thus making their chromaticity values close to zero in the CIELAB color space.[2] Then, the minimum lightness value of the gray-balanced CMY colorant is measured and compared with the lightness values corresponding to the digital values of the black colorant. As soon as the lightness value of the black colorant becomes lower than the minimum lightness value of the gray-balanced CMY colorants, the black colorant begins to be used to reproduce denser blacks, and the amounts of the CMY colorants slowly decrease to guarantee the smooth exchange between the gray-balanced CMY colorant and the black colorant due to the slight difference in their perceived gray color. Figure 13 shows the resulting separating path for the gray axis.

In addition, if the input CMY digital value belongs to a gray region, the input CMY digital value is separated into the weighed sum of the separated CMYLcLm digital value and the CMYK digital value on the gray axis. Otherwise, the input CMY digital value is separated into the CMYLcLm digital value to enhance the saturation and dot visibility.

If input CMY digital value belongs to a gray region

$$\begin{bmatrix} C' \\ M' \\ Y' \\ K' \\ Lc' \\ Lm' \end{bmatrix} = \left(1 - \frac{\alpha}{TH_b}\right) \cdot \begin{bmatrix} C \\ M \\ Y \\ K \\ 0 \\ 0 \end{bmatrix} + \frac{\alpha}{TH_b} \cdot \begin{bmatrix} C \\ M \\ Y \\ 0 \\ Lc \\ Lm \end{bmatrix}, \quad (9)$$

else

$$C'M'Y'K'Lc'Lm' = CMYLcLm$$

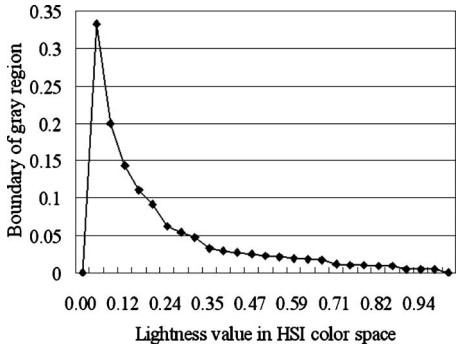


Figure 14. Boundary of the gray regions in HSI color space.

where $\alpha$ represents the weight related to the value of the saturation; $TH_b$ is the threshold value that indicates the boundary of the gray regions and can be expressed as the value of the saturation in the hue, saturation, and intensity (HSI) color space depending on the lightness value. To determine the boundary of the gray regions, the gray digital values sampled by ten are generated, and the digital values are individually increased by a fixed step size for each channel;

$$C = C_i + \delta \cdot j, \quad M = M_i + \delta \cdot j, \quad Y = Y_i + \delta \cdot j, \qquad (10)$$

where $C_i$, $M_i$, and $Y_i$ indicate the sampled gray digital value. A fixed step size $\delta$ is used to increase the $C_i$, $M_i$, and $Y_i$. The value of $\delta$ is set to three and $j$ changes from 1 from 5. The choices of $i$, $\delta$, and $j$ determine the trade-off between computational cost and optimality of the solution. A set of generated patches for each sampled gray digital value are printed using a digital half-tone. The minimum values showing the appearance of color tones are subjectively determined by the human eye, respectively. Next, the CMY values are inverted to get the RGB values and then transformed into the HSI color space. Their saturation values indicating the boundary of the gray regions are shown in Figure 14. The horizontal axis refers to the lightness values corresponding to gray $R_iG_iB_i$ digital values and vertical axis represents the boundary of gray regions expressed by the saturation values in the HSI color space. The gray regions depend on the lightness values of input RGB values, and the threshold values in dark regions are larger than those in bright regions. With these threshold values indicating the boundary of gray regions, the input CMY digital value is inverted to yield the RGB digital value, and then transformed into the HSI color space. According to its lightness value, the value of $TH_b$ is determined and its saturation value is used as the weight of $\alpha$ in Eq. (9).

## CONSTRUCTION OF LOOK-UP TABLES

The look-up tables are designed to convert the arbitrary input CMY digital values into the CMYKLcLm digital values. In the proposed method, the sampled digital values of cyan and magenta are previously separated into those of CLcLm and MYLm, respectively, to enhance the saturation and the dot visibility. In addition, the sampled gray CMY digital values are again converted into the CMYK digital values using the gray-balancing and GCR to produce better gray reproduction. The sampled input and output digital values forms a pair when stored in three types of look-up tables for cyan, magenta, and gray. Then, an interpolation, such as trilinear, prism, and tetrahedral may be applied to calculate the final CMYKLcLm digital values corresponding to arbitrary input CMY digital values. Therefore, using these look-up tables, an arbitrary input digital value is initially separated into the CMYLcLm digital value from CLcLm and MYLm, and if the input digital value belongs to the predefined gray regions, the input digital value is reconverted into the weighted sum of the CMYK digital value and the separated CMYLcLm digital value.

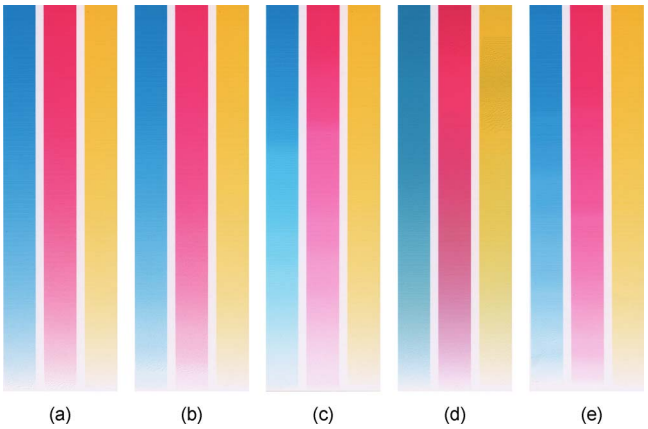


Figure 15. Resulting images for stripe image; (a) CMY color printing, (b) traditional method, (c) Huang's method, (d) Agar's method, and (e) proposed method.

## EXPERIMENTAL RESULTS

For the experiments, an Epson Stylus Photo™ 700 printer was used with a resolution of 360 dpi. To print an input image on the Epson photo-inkjet paper, the monitor characterization was performed by displaying the $9 \times 9 \times 9$ RGB patches on a Sony HS74PL LCD monitor set in the default mode and measuring the CIELAB values using a colorimeter. A tetrahedral interpolation was then used to convert the arbitrary RGB digital values into CIELAB values with a CIE1976 color difference accuracy of less than three for the $4 \times 4 \times 4$ test patches. Next, their CIELAB values were converted into CMY using gamut mapping and backward characterization.[21] The CMY image was then separated into CMYKLcLm using the proposed six-color separation followed by the scalar error diffusion half-toning.

## STRIPE AND NATURAL IMAGE EXPERIMENT

First, the "stripe" image was chosen to test the performance of four six-color separation methods without gamut mapping. The images that resulted from CMY color printing, six-color separation using the color difference, six-color separation using the lightness and subjective granularity, Agar's method,, and the proposed six-color separation are shown in Figure 15 for cyan, magenta, and yellow. In Fig. 15(b), it was shown that the printed dots with the satu-

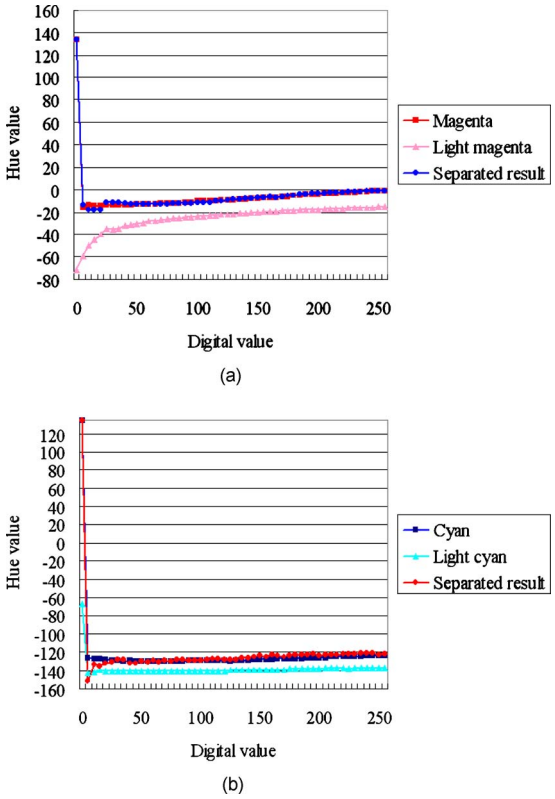


Figure 16. Hue values; (a) magenta, light magenta, and separated result of magenta and (b) cyan, light cyan, and separated result of cyan.

rated colorant in the bright regions were very coarse to the human eye, thereby degrading the image quality. Clearly, the use of saturated colorants in the bright regions did not realize the advantage of a six-color printer, which can produce less graininess and great resolution, although the colors of the resulting image were similar to those of input CMY color printing. In Fig. 15(c), it was shown that the reproduced image can be much smoother when only a diluted colorant was used, compared with other methods, as the dot patterns were invisible and pleasant to the human eye. In addition, the resolution in the bright regions seems to be higher than in Figs. 15(a) and 15(b) because the diluted colorant requires more dotted areas to make the same lightness value as that of the saturated colorant. However, the disadvantage was that the reproduced colors were very different from those in CMY color printing, due to the hue difference between the diluted and saturated colorants. Meanwhile, Agar's method included colorimetric errors because the threshold value used for the color difference metric was large, so as to obtain a sufficient number of candidates available on memory. The colors of the resulting images slightly differed from those in CMY color printing. In addition, on the yellow and magenta ramps, the light cyan with a different hue was used in Fig. 15(d), according to the dot visibility orderings, and this heightened the dot visibility. The results of the proposed method that used additional colorants in the bright regions are shown in Fig. 15(e). The use of the additional colorants can reduce the big colorimetric errors seen in Fig. 15(c). The CIE hue values of the diluted colorant,

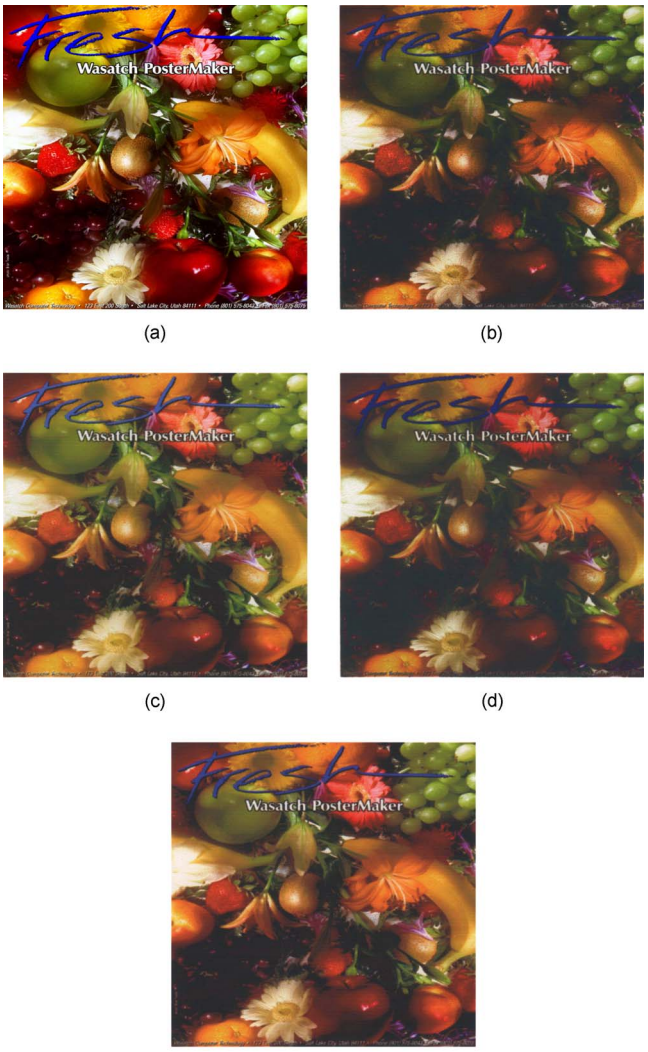


Figure 17. Resulting images for 'Fresh' image; (a) original image, (b) traditional method, (c) Huang's method, (d) Agar's method, and (e) proposed method.

saturated colorant, and the resulting images from the proposed method are compared in Figure 16 for magenta and cyan. By adding an additional colorant to the diluted colorant based on subtractive color-mixing, the hue value of the separated result came close to that of the saturated colorant. Therefore, the proposed method can correct the hue difference in the bright regions. In addition, the dot visibility in Fig. 15(e) also decreased compared to the dots in Figs. 15(b) and 15(d) due to light concentrations of the additional colorants.

Second, the original image and resulting images from the six-color separation methods are shown in Figure 17 for the "Fresh" image. As expected, the traditional six-color separation using the color difference generated a higher dot visibility in the reproduced image, especially for the bunch of grapes and bananas. The use of the saturated colorants in dark regions darkened the image, as shown in Fig. 17(b), even though the tone reproduction was slightly improved. In Fig. 17(c), since the six-color separation using the lightness and subjective granularity used only diluted colorants in the

**Table IV.** Quantitative evaluation of the six-color separation methods for cyan wedges.

| Methods | Color difference | Dot visibility | Total colorant amount |
|---|---|---|---|
| Traditional method | 1.640 | 5.069 | 158 (55%) |
| Huang's method | 6.077 | 3.151 | 171 (60%) |
| Agar's method | 5.854 | 3.672 | 284 (100%) |
| Proposed method | 1.551 | 3.656 | 186 (65%) |

**Table V.** Quantitative evaluation of the six-color separation methods for magenta wedges.

| Methods | Color difference | Dot visibility | Total colorant amount |
|---|---|---|---|
| Traditional method | 1.220 | 4.064 | 200 (68%) |
| Huang's method | 10.06 | 3.016 | 170 (58%) |
| Agar's method | 5.342 | 4.434 | 293 (100%) |
| Proposed method | 1.922 | 2.547 | 196 (66%) |

bright regions, the colors of the resulting image were destroyed. One of the methods of transforming CMY into CMYLcLm, Agar's method, created a darkened image with poor edge sharpness, as shown in Fig. 17(d) due to the maximization of Y, Lc, and Lm. The proposed method used the essential colorants of MYLm and CLcLm to separate magenta and cyan. The lightness of the resulting image was generally brighter than in Fig. 17(d), thus preventing ink wastage. In addition, the use of additional colorants with low dot visibility made it possible to reproduce the image with a smooth dot-pattern and fewer colorimetric errors.

## PERFORMANCE COMPARISON OF VARIOUS SIX-COLOR SEPARATION METHODS

The CIE1976 color difference, the dot visibility, and the total colorant amount were used to compare the performance of various six-color separation methods. The step wedges of magenta and cyan were made based on intervals of five, and their total number was 52. Four six-color separation methods were applied to the step wedges, and then printed with the scalar error diffusion. The CIE1976 color differences between the input cyan wedges and the separated wedges were calculated. The dot visibility was calculated as the standard deviation of the lightness in the SCIELAB space for the scanned step wedges. The Epson Perfection V700 scanner was used at the 200 dpi mode. The total colorant amount was defined as the sum of the separated digital values per pixel in the step wedge. The average color difference, the dot visibility, and the total colorant amount are shown in Tables IV and V for cyan and magenta, respectively.

As might be expected, the six-color separation using the lightness and subjective granularity showed a very small dot visibility, yet its color difference was quite high, whereas opposite results were obtained for the six-color separation using the color difference. In the traditional method, even if the total amounts of colorants are small, ink spreading can be a little happened due to the use of the saturated colorant with dark concentration in the dark regions. In Agar's method, the maximum use of diluted colorants generated a relatively lower dot visibility, but consumed much more colorants than the other methods. In addition, since Agar's method used a large threshold value to get the initial candidates, a larger color difference resulted. The color difference can be further reduced with accurate printer characterization. However, since Agar's method uses all the C, M, Y, K, Lc, and Lm colorants as candidates, the amount of measured data, e.g., number of Neugbauer primaries, is higher than with the proposed method: for YNSN modeling, Agar's method requires 64 measured Neugebauer primaries, while the proposed method uses only eight measured Neugebauer primaries. Thus, if the same amount of measured data were used, the proposed method would produce more accurate YNSN modeling

From the experiment on the dot visibility model, it was predicted that the average dot visibility value of the cyan wedges should be larger than that of magenta wedges, but Agar's method was exceptional. This is because the cyan dots with a different hue were used on the reproduced magenta wedge. The results of the proposed method showed reduced color difference, lower dot visibility, and a low total colorant amount. Since the CLcLm and MYLm colorants were only used to separate the input C and M digital values, wasteful ink consumption was prevented without any constraint, and a sufficient number of candidates was generated in computer memory. Moreover, the use of additional colorants in the bright regions not only reduced significant colorimetric error but also created smooth dot patterns due to light concentration. Furthermore, the model-based printer characterization can be realized easily with reduced three MYLm and CLcLm Neugebauer primaries.

## CONCLUSIONS

This article has proposed a six-color separation method based on a color mixing rule and a quantitative dot visibility metric to reduce the color difference, dot visibility, and total colorant amount. The use of additional colorants and the dot visibility metric according to three types of tonal region produced images with both low dot visibility and a low color difference. In addition, the use of only CLcLm and MYLm prevented excessive colorant use without constraint and generated a sufficient number of candidates in computer memory, providing the opportunity to achieve high color fidelity. Furthermore, the proposed six-color separation method can be extended to eight-color printers, which use two types of light black colorant in addition to CMYKLcLm colorants, while the proposed dot visibility model can be used to find the dot visibility of half-tone patches.

## REFERENCES

[1] G. Sharma, *Digital Color Imaging Handbook* (CRC Press, Boca Raton, FL, 2003).
[2] H. Kang, *Color Technology for Electronic Imaging Devices* (SPIE, Bellingham, WA, 1997).

[3] Y. Noyes, J. Hardeberg, and A. Moskalev, "Linearization curve generation for CcMmYk printing", *Proc. IS&T/SID Eighth Color Imaging Conference* (IS&T, Springfield, VA, 2000) pp. 247–251.
[4] C. Son, Y. Kim, C. Lee, and Y. Ha, "Six color separation for improving graininess in a middle tone region", Proc. SPIE **5293**, 110–120 (2004).
[5] X. Huang and B. Nystrom, "Multi-level ink mixing device and method using diluted and saturated color inks for ink jet printer", US Patent 6,172,692 (2001).
[6] C. Son, Y. Cho, C. Lee, and Y. Ha, "Six color separation using additional colorants and quantitative granularity metric", J. Imaging Sci. Technol. **50**, 25–34 (2006).
[7] M. Shaw, R. Bala, and G. Sharma, "Smooth blending of two inks of similar hue to simulate one ink", Proc. SPIE **5667**, 409–416 (2005).
[8] A. Agar, "Model-based color separation for CMYKcm printing", *Proc. IS&T/SID Ninth Color Imaging Conference* (IS&T, Springfield, VA, 2001) pp. 298–302.
[9] Y. Chen, R. Berns, L. Taplin, and F. Imai, "A multi-ink color separation algorithm maximizing color constancy", *Proc. IS&T/SID Eleventh Color Imaging Conference* (IS&T, Springfield, VA, 2003) pp. 277–281.
[10] Y. Chen, R. Berns, and L. Taplin, "Six color printer characterization using an optimized cellular Yule-Nielsen spectral Neugebauer model", J. Imaging Sci. Technol. **48**, 519–528 (2004).
[11] H. Kang, *Computational Color Technology* (SPIE, Bellingham, WA, 2006).
[12] J. Y. Hardeberg, "Acquisition and reproduction of color images: colorimetric and multispectral approaches", Dissertation.com, USA, 2001.
[13] R. Balasubramanian, "Optimization of the spectral Neugebauer model for printer characterization", J. Electron. Imaging **8**, 156–166 (1999).
[14] I. Amidror and R. Hersch, "Neugebauer and Demichel: Dependence and independence in *n*-screen superpositions for colour printing", Color Res. Appl. **25**, 267–277 (2000).
[15] X. Zhang and B. Wandell, "A spatial extension to CIELAB for digital color image reproduction", Society for Information Display Symposium Technical Digest **27**, 731–734 (1996).
[16] M. Fairchild, *Color Appearance Models* (Wiley and Sons, New York, 2005).
[17] T. Pappas, C. Dong, and D. Neuhoff, "Measurement of printer parameters for model-based halftoning", J. Electron. Imaging **2**, 193–204 (1993).
[18] T. Pappas and D. Neuhoff, "Printer models and error diffusion", IEEE Trans. Image Process. **4**, 66–80 (1995).
[19] G. Johnson and M. Fairchild, "A top down description of S-CIELAB and CIEDE2000", Color Res. Appl. **28**, 425–435 (2003).
[20] D. Tzeng and R. Berns, "Spectral-based ink selection for multiple-ink printing II. Optimal ink selection", *Proc. IS&T/SID's Seventh Color Imaging Conference* (IS&T, Springfield, VA, 1999) pp. 182–187.
[21] C. S. Lee, C. H. Lee, and Y. H. Ha, "Parametric gamut mapping algorithms using variable anchor points", J. Imaging Sci. Technol. **44**, 68–73 (2000).